Color Normalization Approach to Adjust Nuclei Segmentation in Images of Hematoxylin and Eosin Stained Tissue

Adam Piórkowski[1] and Arkadiusz Gertych[2]

[1] Department of Geoinfomatics and Applied Computer Science
AGH University of Science and Technology,
A. Mickiewicza 30 Av., 30–059 Cracow, Poland,
[2] Department of Surgery, Department of Pathology and Laboratory Medicine
Cedars-Sinai Medical Center, Los Angeles, CA 90048, USA,
pioro@agh.edu.pl

Abstract. Lack of standards in hematoxylin and eosin (H&E) tissue staining across laboratories is one of the reasons for differences in appearance of specimens under the microscope. It also negatively impacts the performance of digital image analysis algorithms, including nuclei segmentation that is deemed to be affected the most. To alleviate this problem, we searched through the color space to find color targets to which coloration of the original H&E image can be transferred with the goal to improve performance of a baseline nuclear segmentation method. Color targets that we found were plugged into the Reinhard's color normalization algorithm to transfer the original H&E image to a new color space. The color-transferred images were then processed by two proposed approaches that subtract and subsequently threshold red and blue color channels. Implementation of these steps improved the amount of false positive pixels and splitting of clustered nuclei in the nuclear mask generated by the baseline method. The pixel-based segmentation accuracy was 94% in selected images. The performance was assessed in heterogeneous images of colon with manually delineated nuclei[3].

Keywords: edge detection, nuclei segmentation, cell counting, image processing, color transfer, microscopy images

[3]This is the manuscript of:

Piorkowski, A, Gertych, A: Color Normalization Approach to Adjust Nuclei Segmentation in Images of Hematoxylin and Eosin Stained Tissue. Springer, AISC, vol. 762, 2019, pp. 393-406.

The final authenticated version is available online at https://doi.org/10.1007/978-3-319-91211-0_35 .

1 Introduction

Hematoxylin and eosin (H&E) are dyes that are commonly used in tissue staining for histological evaluation. H&E staining cocktail is largely not standardized and often inconsistent across laboratories. The inconsistency that is caused by different quality and freshness of the staining reagents can create variability in contrast and coloration that is an impediment to quantitative digital imaging.

The lack of standardized protocols for H&E staining results in profound differences in coloration of specimens. Depending on reagents' concentration, the appearance of cell nuclei can range from pale to dark blue. Likewise, discrepancies in concentration of eosin will result in cytoplasm staining with a wide range of pink, red, violet or orange. The issue of differences in tissue coloration negatively affects performance of nuclei segmentation algorithms [19].

Despite this disadvantage, the majority of approaches targeting the segmentation of nuclei in images of H&E stained tissues is based on the analysis of blue image channel because blue color approximates the location of hematoxylin and it is easy to work with . More sophisticated approaches utilize red and blue color ratio [1], a gray-level image representation [7, 10], or ad-hoc color standardization [5]. In [20] the authors concluded that a substantial overlap exists in the color un-normalized images, but the normalization helps to discern images components such as nuclei, cytoplasm and background. However, no quantitative data was shown that color normalization improves analytically routines such as for example segmentation of nuclei.

Other methods put more emphasis on color normalization in the image followed by the deconvolution of hematoxylin, eosin or other stains, and then use the hematoxylin image as a starting point for nuclear segmentation [2, 6, 16]. Color normalization methods have been developed to alleviate the problem of inconsistencies in the preparation of histology slides. The goal is to bring images of slides that were processed under different conditions into unified space to enable robust quantitative tissue analysis. Reinhard's [17], Macenko's [9], and Li's [8] color normalization methods that were compared in [6] seem to be most commonly used. A review of these and other state-of-the-art color normalization methods can be found in [14].

With regards to nuclei segmentation methods that utilize blue, red, or both channels for input, as well as color-normalization in the image processing pipeline, there seems to be an unexplored opportunity in manipulating basic color channels that could lead to a more optimal separation of dyes in the image. In this work, we propose three computationally inexpensive approaches for finding optimal vectors of Lab color space to which original image colors can be transferred by means of the Reinhard's algorithm [17]. We check whether the analytically determined vectors have the potential to separate tightly packed nuclei which a baseline segmentation has difficulties to deal with.

Segmentation of cell nuclei in tissues with clusters of heterogeneous cells is a long-standing problem in quantitative image analysis [13]. For our research, we chose colon tissue because epithelial cells in colon crypts are tightly packed and have elliptical or cone shapes. In addition, stroma that surrounds the crypts,

consists of fibroblasts, nerve and blood vessel cells, and cells of immune system that all have different size and morphology.

2 Materials

One glass slide with normal colon specimen was retrieved from the Biobank at Cedars-Sinai Medical Center, then stained with hematoxylin and eosin (H&E) and subsequently digitized with Aperio AT Turbo (Leica Biosystems, Vista CA) whole slide scanner. The scanning magnification was set to 40x and the pixel size was 0.244μm$\times 0.244\mu$m. Next, the digital slide outputted by the scanner was reviewed by a pathologist who identified heterogenous tissue areas containing epithelium with adjacent stroma and immune cells. Then, square tiles (n=80) with the tile length of 1000 pixels were manually selected and extracted from the digital slide, and saved as 8-bit encoded RGB matrices for further analysis.

3 Methods

3.1 Baseline Segmentation of Nuclei

H&E images (Fig. 1(a)) were subjected to Reinhard's color normalization [17], and then color-deconvoluted to obtain a gray scale image of the hematoxylin staining (Fig. 1(b)). We chose the Reinhard's method over other methods available from the literature due to its low computational complexity. The hematoxylin image was subsequently filtered with a circular averaging filter (pillbox) with an experimentally adjusted radius=5 to attenuate noise and remove small non-nuclear objects. The image was automatically binarized using the statistical dominance algorithm (SDA) [12,15]. In this method, the intensity threshold and the radius parameters were respectively set to 90 and 50. Separately, the filtered hematoxylin image was processed by the fast radial symmetry transform (FRST) to yield an intensity image in which nuclear centers are marked by high-intensity peaks. Next, the FRST image was thresholded to obtain a binary mask of nuclear markers, and a marker-controlled watershed transform was applied to separate clustered and closely positioned nuclei (Fig. 1(c)). The watershed lines were traced within the mask of nuclei using the hematoxylin image that served as an intensity landscape to find ridge lines between marked nuclei similarly to the procedure described in [4]. Parameters for the FRST were set as described in [3]. All other parameters were determined experimentally to render best nuclear delineation performance. In the next step, original images with superimposed segmentation results (Fig. 2(a)) were shown to a pathologist who reviewed and then manually corrected the contours of segmented nuclei. This activity was limited only to correcting over- and under-segmentations (Fig. 2(b)). This manually corrected mask served as a ground truth for evaluation of methods discussed in the subsequent sections.

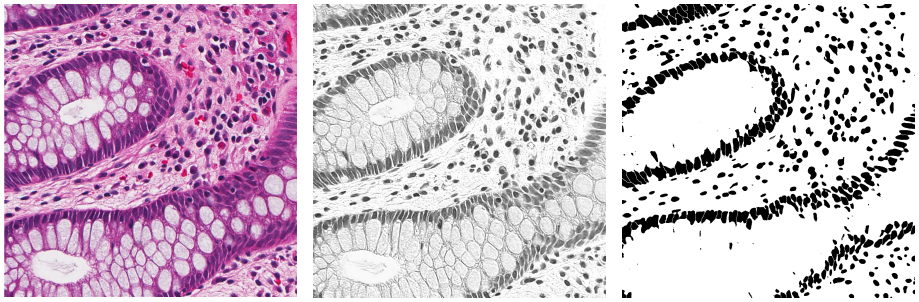

(a) (b) (c)

Fig. 1. Processing steps of baseline segmentation of nuclei: (a) original H&E image, (b) color-deconvoluted hematoxylin channel, and (c) baseline mask of nuclei

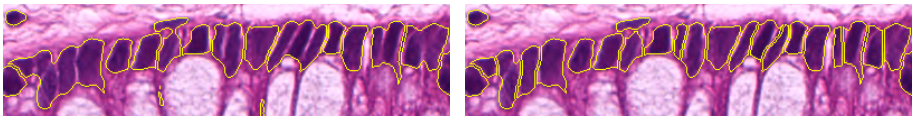

(a) (b)

Fig. 2. A closeup view of nuclear segmentation results: (a) baseline method, (b) manual refinement of the baseline segmentation

3.2 Analysis of Dependencies Between Colors in H&E Stained Images

To highlight the possibilities of improving segmentation performance through the analysis of color channels, one can consider an example in Figure 3 that shows the color intensity along profiles in the original image (Fig. 3(a)) and the same image normalized using Reinhard's method [17] (Fig. 3(b)). In this example, the set of normalization parameters in the Lab space, calculated from the RGB space is as follows (mean,std): (L=(198,78), a=(120,9), b=(185,3)). The profiles show color brightness values in each color channel. One can note that in the original image blue is the most intense color in cell nuclei, but this is not the case for the color-normalized image in which blue color in nuclei has reduced intensity.

However, one can notice that the difference in pixel intensities between red and blue channels is the most prominent at the edge between the nucleus and surrounding cytoplasm. More specifically, examining the relationships between intensities in the red (R) and blue (B) channels opens up the possibility of detecting nuclear boundaries, for instance by applying the following formula:

$$V_1(x, y) = |R(x, y) - B(x, y)| \tag{1}$$

This concept is visualized in Fig. 4(b). Following this idea, pixels that are located at nuclear edges visualized through Equ. (1) can be considered as local image minima.

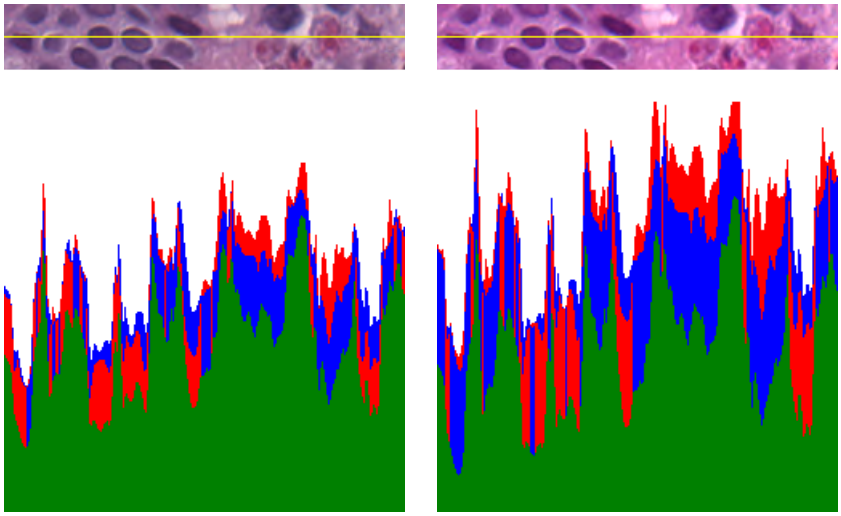

(a) original (b) color-normalized

Fig. 3. Image profiles across the original and color normalized H&E images. The normalization enhances blue and red colors and attenuates the green color. Note that red and blue colors are much more intense than the green color. Interestingly, the color normalization reduced the intensity of blue color which in some areas is less intense than red color. Intensity value is reflected vertically

Unfortunately, the obtained result in Figure 4(b) may be difficult to use for extracting nuclear borders due to poor foreground to background ratio. Instead, full nuclei can be marked, taking into account only those areas in which the intensity of the red color dominates over the blue color. This leads to an extended version of formula Equ. (1) defined as follows:

$$V_2(x,y) = \max\left(0, B\left(x,y\right) - R\left(x,y\right)\right) \tag{2}$$

3.3 Seeking Optimal Color-Normalization Parameters Through a Random Guess

A test was carried out to evaluate approach described by Equ. (2). Three randomly selected original H&E images of colon tissue (see Sec. 2), marked here as P1, P2 and P3, were color-normalized each using 100,000 randomly generated vectors with mean and stds of Lab color space components, and colors in the original image were transferred accordingly. The ranges of color means ranged from 0 to 255, and the std deviation from 0 to 500. Following this step, a nuclear mask was obtained by thresholding of the image $V_2(x,y)$ (Fig. 4(c)) with a threshold of t=1 separating nuclei (values under the threshold) from other components. Example result is show in Fig. 5(b). Then, the nuclear mask was

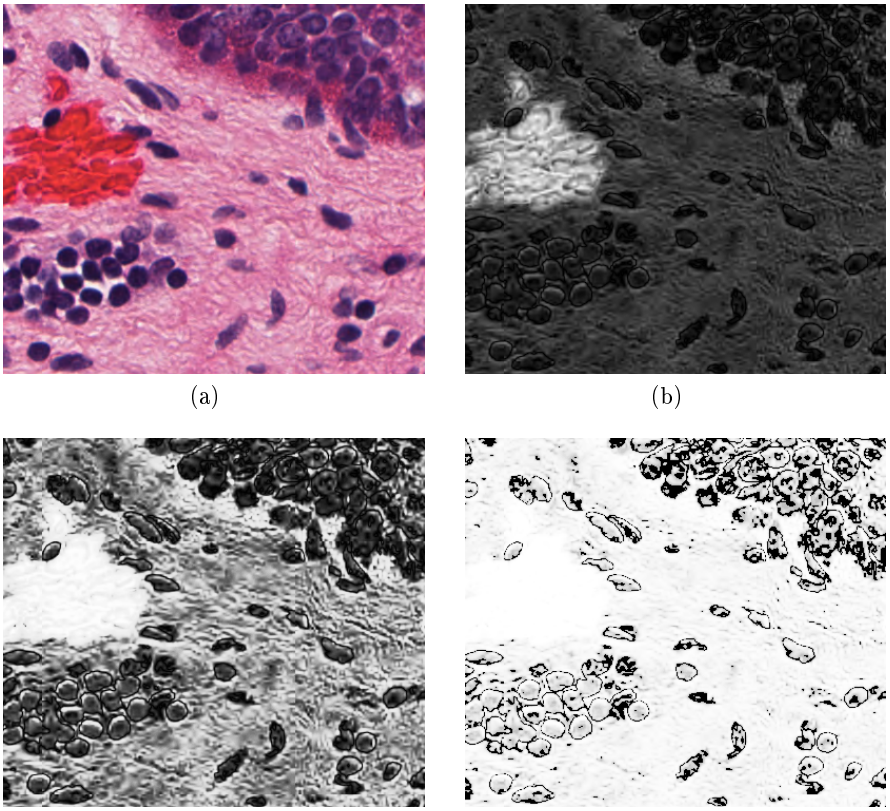

Fig. 4. Example output from the method described by Equ. (1). After processing the original H&E image from (a), the output in (b) is histogram stretched (c), and additionally gamma-corrected (γ=4.5) (d) to visualize edges between nuclei and cytoplasm (black lines) that the Equ. (1) enhances

overlaid onto the corresponding ground-truth image to assess the segmentation accuracy.

The segmentation performance of this approach was examined using the following measures: Dice coefficient (known also as F1 score), accuracy (ACC), and accuracy with 5× penalty rate for FP detections (FPEN5) see Tab. 1. The FPEN5 is a modification of the original ACC measure, and is defined solely for the purpose of this project. It penalizes stronger the presence of FP pixels in the output mask. Thus, FPEN5 is helpful in finding Lab parameters that lead to a reduces number of FP instances. The measures were calculated using the ground truth and the output mask based on a 2×2 confusion matrix.

This method selects Lab vectors that maximize the measures of accuracy. However, its main disadvantage is the high computational cost. This cost is pre-

Table 1. Measures of nuclei segmentation performance

abbr.	DICE	ACC	FPEN5
name	DICE Coefficient	ACCURACY	FP PENALTY 5
formula	$\frac{2 \cdot TP}{2 \cdot TP + FP + FN}$	$\frac{TP + TN}{TP + TN + FP + FN}$	$\frac{TP + TN}{TP + TN + 5 \cdot FP + FN}$

Table 2. Performance of nuclear segmentation by method Equ. (2) with color transfer parameters (ctv) in the Lab space determined by a random guess. Best parameters are presented along the performance measures

Image	DICE	ACC	FPEN5
P1	0.8734	0.9615	0.9385
@ctv	(31,488), (15,281), (135,341)	(249,120), (99,474), (242,44)	(244,30), (245,142), (215,122)
P2	0.8676	0.9453	0.9134
@ctv	(220,29), (123,490), (46,79)	(220,29), (123,490), (46,79)	(234,6), (90,23), (123,56)
P3	0.8995	0.9537	0.9119
@ctv	(255,20), (48,275), (227,228)	(251,10), (196,117), (97,261)	(252,54), (235,40), (100,51)

dominantly associated with transferring colors in the original image to the new space (100,000 iterations), and then generating the nuclear mask. This process took 8h for a code written in Matlab R2017a (Matlab, Natick MA). Nevertheless, the search through a random guess provides some hints that Lab parameters leading to a high segmentation accuracy can be found experimentally. In the future studies we will implement an approach that determines optimal Lab parameters analytically. Preliminary results included in Tab. 2 are quite diverse, and suggest that the range of vector components is rather wide - spreading nearly through the entire range of possible values of the mean in each channel (0–255).

3.4 Analysis of Red Channel After Custom Color Transformations

In the previous section we demonstrated the feasibility of the experiments and provide a proof of concept for the method. In this section we narrow down our analysis to the R channel by taking into account the following function:

$$V_3(x,y) = \begin{cases} 0, R(x,y) > 0 \\ 1, R(x,y) = 0 \end{cases} \tag{3}$$

To assess the applicability of this method, we used the color-transformed images from the previews experiment and then applied Equ. (3) to obtain the nuclear mask. Example images for the highest measures of accuracy are presented in Fig. 6. The highest measures with the corresponding Lab vectors are included in Table 3. Based on this experiment, we conclude that this method yields very similar results to those that are based on the $V_2(x,y)$ output. However, we find that segmentation results from the method based on $V_3(x,y)$ not only rank among the best, but they also lead to a single and generally applicable Lab vector = ((255, 400) (0, 0) (0, 20)) found for the P3 image (Tab. 4 and 5).

Figure 7 shows example results of nuclear mask outputted by $V_3(x,y)$ for the images color-normalized with these Lab parameters to arrive at highest FPEN5,

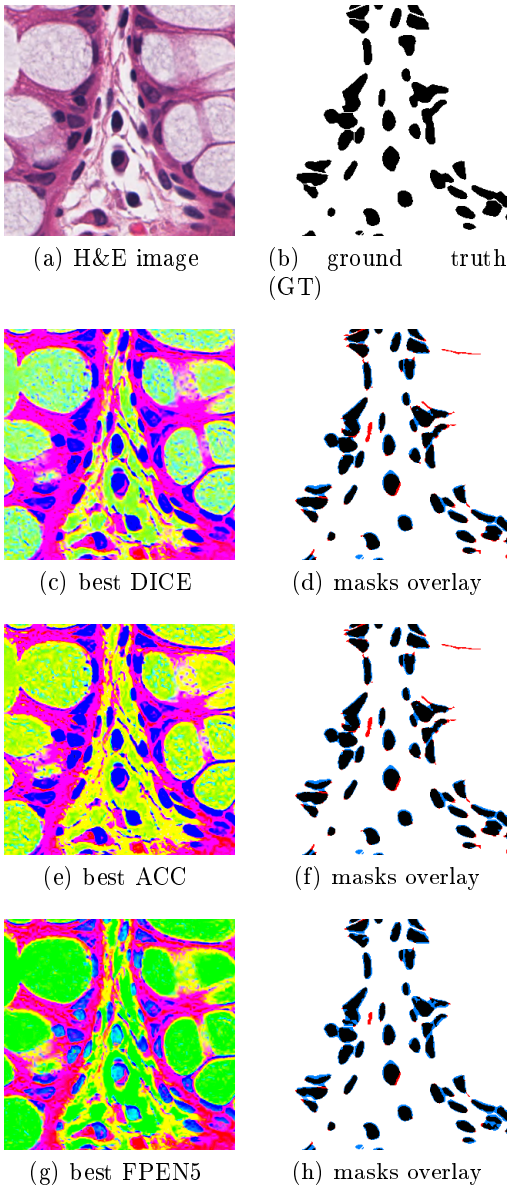

(a) H&E image (b) ground truth (GT)

(c) best DICE (d) masks overlay

(e) best ACC (f) masks overlay

(g) best FPEN5 (h) masks overlay

Fig. 5. Example nuclear segmentations in color transferred H&E images. The original image from (a) was color-transferred using three different Lab vectors and subsequently segmented using Equ. (2). Each of the Lab vectors maximizes respectively the DICE (c), ACC (e) and FPEN5 (g) performance segmentation measures. The difference between ground truth (GT) nuclear mask in (b) and the segmentation results for each measure is respectively shown in (e), (f), and (h). TP pixels are black, FP red, and FN blue

ACC, and Dice measures. Figure 7(d) shows that objects in the outputted mask and ground-truth mask overlap (black color). Discordant pixels are marked with blue (FN) or red colors (FP) respectively. Interestingly, when we take a closer look at the red lines in Figures 6(d), 6(f), 6(h) we notice that they divide closely adjacent nuclei. In addition, blue areas - nuclei or their fragments that were removed by the baseline method are highlighted. This suggests that the proposed method incorporates missing pixels and removes those that do not belong to nuclei.

From results in Table 4 and Table 5, we glean that both manual and automated methods overlap in a narrow range color transfer vectors. Interestingly, the mean and std values for the component a of the Lab color space, as well as the mean for the component b can be set to 0. This observation can be helpful in implementation of less complex algorithms that seek optimal color transfer vectors.

Table 3. Performance of nuclear segmentation by method Equ. (3) with color transfer parameters (ctv) in the Lab space determined by a random guess. Best parameters are presented together with corresponding the measures

Image	DICE	ACC	FPEN5
P1	0.8657	0.9579	0.9298
@ctv	(213,460), (223,80), (68,21)	(248,485), (63,80), (14,22)	(94,131), (2,6), (132,5)
P2	0.8723	0.9448	0.9036
@ctv	(213,452), (120,145), (78,31)	(125,238), (87,48), (157,16)	(208,237), (54,3), (207,19)
P3	0.8981	0.9528	0.9117
@ctv	(231,432), (194,137), (26,30)	(222,385), (188,154) (182,27)	(251,336), (31,107), (130,14)

Table 4. Performance of the baseline nuclear segmentation method preceded by the manual adjustment of color transfer vectors. Note, that it is possible to find more than one vector that leads to high values of DICE, ACC, and FPEN5. These vectors rank in the top 30 vectors out of 100,000 that were found by a random guess

Image	color transfer vector	Dice	ACC	FPEN5
P1	(255,400), (0,0), (0,20)	0.8284	0.9513	0.9272 (22 of 100 000)
P1	(255,320), (0,0), (0,20)	0.7609	0.9371	0.9260 (38 of 100 000)
P2	(255,300), (0,0), (0,20)	0.7885	0.9226	0.9031 (3 of 100 000)
P2	(255,300), (0,0), (0,30)	0.8161	0.9304	0.9028 (8 of 100 000)
P3	(255,360), (0,0), (0,25)	0.8579	0.9403	0.9104 (28 of 100 000)
P3	(255,360), (0,0), (0,20)	0.8428	0.9352	0.9103 (30 of 100 000)

4 Summary

Challenges of nuclei segmentation in colon tissue have previously been recognized in [11,16,18,19,21–23]. For our research, we chose colon tissue because epithelial

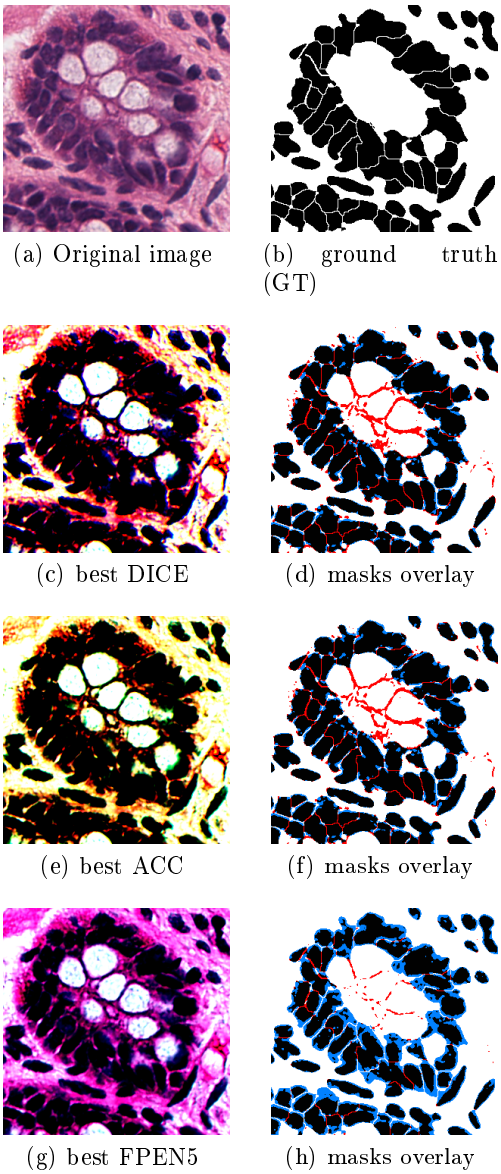

(a) Original image (b) ground truth (GT)

(c) best DICE (d) masks overlay

(e) best ACC (f) masks overlay

(g) best FPEN5 (h) masks overlay

Fig. 6. Example nuclear segmentations in color transferred H&E images. The original image from (a) was color-transferred using three different Lab vectors and subsequently segmented using Equ. (3). Each of the Lab vectors maximizes respectively the DICE (c), ACC (e) and FPEN5 (g) performance segmentation measures. The difference between ground truth (GT) nuclear mask in (b) and the segmentation results for each measure is respectively shown in (d), (f), and (h). TP pixels are black, FP red, and FN blue

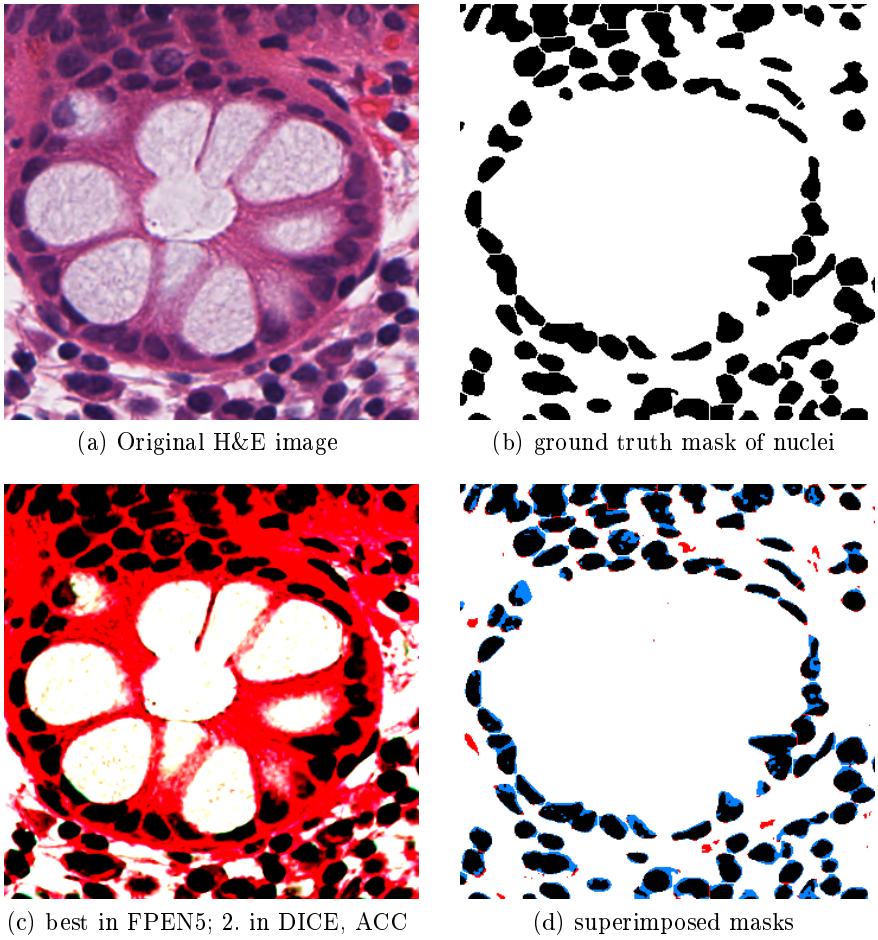

(a) Original H&E image (b) ground truth mask of nuclei

(c) best in FPEN5; 2. in DICE, ACC (d) superimposed masks

Fig. 7. An example of manual adjustment of color-transfer parameters to maximize DICE, ACC and FPEN performance measures. The meaning of colors in (d) is the same as in Figures 5 and 6

cells in colon crypts are tightly packed and have elliptical or cone shapes. In addition, stroma that surrounds the crypts, consists of fibroblasts, nerve and blood vessel cells, and cells of the immune system that have different size and morphology.

Our experiments were conducted using a lab-grown nuclei segmentation algorithm applied to high-resolution images of colon crypts that were supplemented with pathologist ground truth annotations. For three images that we randomly selected from our data set, our experimental approaches yielded target Lab color space vectors to which the images were normalized with and lead to a more accurate nuclei segmentation as compared to a method (see Materials) that has implemented an ad hoc color normalization vector. Our color normalization

Table 5. Performance of the baseline nuclear segmentation method preceded by the manual adjustment of color transfer vectors for a single image in a selected range of values. Results from row 10 are visualized in Figure 7

Image	color transfer vector	Dice	ACC	FPEN5
P3	(255,300), (0,0), (0,10)	0.6586	0.8814	0.8770
P3	(255,300), (0,0), (0,15)	0.7336	0.9015	0.8934
P3	(255,300), (0,0), (0,20)	0.7809	0.9155	0.9035
P3	(255,300), (0,0), (0,25)	0.8133	0.9256	0.9087
P3	(255,300), (0,0), (0,30)	0.8350	0.9326	0.9095
P3	(255,360), (0,0), (0,5)	0.7440	0.9043	0.8931
P3	(255,360), (0,0), (0,10)	0.7915	0.9185	0.9027
P3	(255,360), (0,0), (0,15)	0.8226	0.9285	0.9086
P3	(255,360), (0,0), (0,20)	0.8428	0.9352	0.9103
P3	(255,360), (0,0), (0,25)	0.8579	0.9403	**0.9104**
P3	(255,400), (0,0), (0,20)	**0.8650**	**0.9425**	0.9064
P3	(255,400), (0,0), (0,100)	0.7317	0.8471	0.5577
P3	(255,520), (0,0), (0,100)	0.8470	0.9230	0.7478
P3	(255,520), (0,0), (0,120)	0.7228	0.8362	0.5282
P3	(255,520), (0,0), (0,140)	0.6545	0.7742	0.4227

approaches relied on the Reinhard's method which has low computational complexity and allows manipulating components of the Lab color spaces. The ability to directly manipulate Lab parameters is the main advantage of the proposed methods over many others published to date.

Following the normalization, the images were processed by the proposed approaches that in principle subtract one color channel from another or threshold the red channel in post-normalized images. These experiments led to a segmentation accuracy of 94% or better depending on the method.

5 Further Work

Our results indicate that by manipulating color spaces in the image is advantageous for the nuclei segmentation procedure. We found numerous vectors that led to highly accurate segmentation. However, finding one common Lab vector or a small set of vectors for all images would be the ultimate goal. Further work should consider a more thorough search of Lab vectors, particularly for the methods described with Equ. (2) and Equ. (3) because they have the highest potential of separating clustered cells.

Acknowledgement. This work was financed by the AGH – University of Science and Technology, Faculty of Geology, Geophysics and Environmental Protection as a part of a statutory project. The authors would like to thank Dr. Karolina Nurzynska for using her software to generate data for this research.

References

1. Chang, H., Han, J., Borowsky, A., Loss, L., Gray, J.W., Spellman, P.T., Parvin, B.: Invariant delineation of nuclear architecture in glioblastoma multiforme for clinical and molecular association. IEEE Transactions on Medical Imaging **32**(4), 670–682 (2013)
2. Cui, Y., Hu, J.: Self-adjusting nuclei segmentation (SANS) of hematoxylin-eosin stained histopathological breast cancer images. In: IEEE International Conference on Bioinformatics and Biomedicine (BIBM), 2016, pp. 956–963. IEEE (2016)
3. Gertych, A., Joseph, A.O., Walts, A.E., Bose, S.: Automated detection of dual p16/ki67 nuclear immunoreactivity in liquid-based Pap tests for improved cervical cancer risk stratification. Annals of Biomedical Engineering **40**(5), 1192–1204 (2012)
4. Gertych, A., Ma, Z., Tajbakhsh, J., Velásquez-Vacca, A., Knudsen, B.S.: Rapid 3-d delineation of cell nuclei for high-content screening platforms. Computers in Biology and Medicine **69**(Supplement C), 328 – 338 (2016)
5. Kłeczek, P., Dyduch, G., Jaworek-Korjakowska, J., Tadeusiewicz, R.: Automated epidermis segmentation in histopathological images of human skin stained with hematoxylin and eosin. In: Medical Imaging 2017: Digital Pathology, vol. 10140, p. 101400M. International Society for Optics and Photonics (2017)
6. Kłeczek, P., Mól, S., Jaworek-Korjakowska, J.: The accuracy of H&E stain unmixing techniques when estimating relative stain concentrations. In: Polish Conference on Biocybernetics and Biomedical Engineering, pp. 87–97. Springer (2017)
7. Kowal, M., Filipczuk, P., Obuchowicz, A., Korbicz, J., Monczak, R.: Computer-aided diagnosis of breast cancer based on fine needle biopsy microscopic images. Computers in Biology and Medicine **43**(10), 1563–1572 (2013)
8. Li, X., Plataniotis, K.N.: A complete color normalization approach to histopathology images using color cues computed from saturation-weighted statistics. IEEE Transactions on Biomedical Engineering **62**(7), 1862–1873 (2015)
9. Macenko, M., Niethammer, M., Marron, J., Borland, D., Woosley, J.T., Guan, X., Schmitt, C., Thomas, N.E.: A method for normalizing histology slides for quantitative analysis. In: IEEE International Symposium on Biomedical Imaging, ISBI'09., pp. 1107–1110. IEEE (2009)
10. Mazurek, P., Oszutowska-Mazurek, D.: From the Slit-Island Method to the Ising model: analysis of irregular grayscale objects. International Journal of Applied Mathematics and Computer Science **24**(1), 49–63 (2014)
11. Nawandhar, A.A., Yamujala, L., Kumar, N.: Image segmentation using thresholding for cell nuclei detection of colon tissue. In: International Conference on Advances in Computing, Communications and Informatics (ICACCI), 2015, pp. 1199–1203. IEEE (2015)
12. Nurzynska, K., Mikhalkin, A., Piorkowski, A.: CAS: Cell Annotation Software - research on neuronal tissue has never been so transparent. Neuroinformatics **15**, 365–382 (2017)
13. Nurzynska K.: Deep Learning as a Tool for Automatic Segmentation of Corneal Endothelium Images. Symmetry **10**(3), 60 (2018)
14. Onder, D., Zengin, S., Sarioglu, S.: A review on color normalization and color deconvolution methods in histopathology. Applied Immunohistochemistry & Molecular Morphology **22**(10), 713–719 (2014)
15. Piorkowski, A.: A statistical dominance algorithm for edge detection and segmentation of medical images. In: Information Technologies in Medicine, *Advances in Intelligent Systems and Computing*, vol. 471, pp. 3–14. Springer (2016)

16. Qin, Y., Walts, A.E., Knudsen, B.S., Gertych, A.: Computerized delineation of nuclei in liquid-based pap smears stained with immunohistochemical biomarkers. Cytometry Part B: Clinical Cytometry **88**(2), 110–119 (2015)
17. Reinhard, E., Adhikhmin, M., Gooch, B., Shirley, P.: Color transfer between images. IEEE Computer Graphics and Applications **21**(5), 34–41 (2001)
18. Rogojanu, R., Bises, G., Smochina, C., Manta, V.: Segmentation of cell nuclei within complex configurations in images with colon sections. In: IEEE International Conference on Intelligent Computer Communication and Processing (ICCP), 2010, pp. 243–246. IEEE (2010)
19. Veta, M., van Diest, P.J., Kornegoor, R., Huisman, A., Viergever, M.A., Pluim, J.P.: Automatic nuclei segmentation in H&E stained breast cancer histopathology images. PLOS ONE **8**(7), e70,221 (2013)
20. Zarella, M.D., Yeoh, C., Breen, D.E., Garcia, F.U.: An alternative reference space for H&E color normalization. PLOS ONE **12**(3), 1–14 (2017)
21. Chen, J.M., Li, Y., Xu, J., Gong, L., Wang, L.W., Liu, W.L., Liu, J.: Computer-aided prognosis on breast cancer with hematoxylin and eosin histopathology images: A review. Tumor Biology **39**(3), 1010428317694,550 (2017)
22. Eramian, M., Daley, M., Neilson, D., Daley, T.: Segmentation of epithelium in h&e stained odontogenic cysts. Journal of microscopy **244**(3), 273–292 (2011)
23. Tosta, T.A.A., Neves, L.A., do Nascimento, M.Z.: Segmentation methods of h&e-stained histological images of lymphoma: A review. Informatics in Medicine Unlocked **9**, 35–43 (2017)